Quantifying Soil Structure and Preferential Flow in Intact Soil Using X-ray Computed Tomography

Lifang Luo
Henry Lin*

Dep. of Crop and Soil Sciences
116 ASI Bldg.
Pennsylvania State Univ.
University Park, PA 16802

Phil Halleck

Dep. of Energy & Geo-Environmental Eng.
152 Hosler Bldg.
Pennsylvanai State Univ.
University Park, PA 16802

Computed tomography (CT) provides a nondestructive means of observing soil structure and monitoring solute breakthrough in real time. We investigated an intact soil column 10 cm in diameter and 30 cm in length using industrial CT with a resolution of 105.5 by 105.5 by 125.25 μm. The satiated soil column was scanned to obtain overall soil structure. Then 60 g L^{-1} KI solution was injected at 6.6 mL min^{-1} for about 23 h and solute transport was monitored in real time by scanning two critical positions in the column and taking digital radiographs. At the end of the experiment, the whole column was scanned again to obtain the overall solute mass distribution. The voxel-based soil porosity and solute concentration were quantified. The three-dimensional visualization of the pore network and solute distribution with time showed that both the pore network and the flow pattern varied considerably with soil depth, in part due to the soil horizonation and different macropores involved. Although the macroporosity below the Ap1 horizon was much lower, macropores were more continuous and less tortuous as a result of limited agricultural disturbance and more earthworm activities. Only part of the macropores at the subsurface were effective, however, in transporting the solute. The results revealed a sequential initialization of the transport process from the macropore domain to the matrix domain and a decreased degree of interaction between the two domains with soil depth. Point-specific breakthrough curves were obtained from real-time point-specific solute concentration and porosity, from which point-specific pore velocity was determined. Preferential flow pathways in this intact structured soil consist of a complex network of earthworm burrows, root channels, interaggregate macropores, and mesopores or even micropores in the soil matrix. Modeling of this flow network and its dynamics requires a new approach different from the classical continuous-domain approach.

Abbreviations: CT, computed tomography; DR, digital radiograph.

Soil structure is critical to water movement and solute transport, as bypass flow along soil structural units (such as interpedal macropores or wormholes) can move chemicals preferentially to a deeper depth at a faster rate (Beven and Germann, 1982; Chen, 1992; Perret et al., 2000). Although constituting only a small percentage of total soil porosity, macropores may dominate near-saturated flow flux under certain circumstances (Luxmoore et al., 1990). In such cases, traditional models of water movement and solute transport for homogeneous soils do not provide an adequate description of the processes involved. Various models for estimating water flow and solute transport in structured soils have been developed. Feyen et al. (1998) reviewed both deterministic and stochastic approaches to quantitatively describe water flow and solute transport in heterogeneous soils. Šimunek et al. (2003) reviewed and compared existing deterministic models to estimate preferential or nonequilibrium flow and transport in the vadose zone. These mod-

els include the dual-porosity model (van Genuchten and Wierenga, 1976), the dual-permeability model (Gerke and Schaap, 1993), the multiregion model (Gwo et al., 1995), the kinematic wave model (Germann, 1985), and others. Preferential flow dynamics and their relation to soil structure have not yet been fully understood, however, prohibiting reliable estimate of water flow and solute movement in structured soils. Beven and Germann (1982) stated that data on the structure of macropore systems, the nature of macropore flow, and the interactions between macropores and matrix were extremely lacking. This lack of detailed and quantitative relationships between soil structure (including macropores) and preferential flow dynamics continues even today (Lin et al., 2005; Šimunek et al., 2003; Köhne and Mohanty, 2005).

It is recognized that experimental measurement and accurate quantification of soil structure and preferential flow pose significant challenges. Traditionally, soil structure has been described by pedologists using in situ morphological descriptions or thin sections in the laboratory, and by soil physicists using wet and dry sieving to measure the percentage of water-stable aggregates; however, these methods cannot provide an adequate surrogate for undisturbed structure (Young et al., 2001). On the other hand, the pore network, especially pore size distribution and connectivity, is believed to control soil hydraulic properties (Vogel, 2000; Perret et al., 2000; Pierret et al., 2002). Research into the linkage between undisturbed soil structure and real-time flow dynamics is needed.

Destructive methods have been used to observe preferential flow, particularly in combination with various dye tracers (Feyen

et al., 1999; Flury and Wai, 2003). Indirect methods of collecting leachate through the soil either by gravity (e.g., zero-tension pan lysimeters) or by applying a capillary suction (e.g., wick lysimeters) have also been used to study preferential flow (Boll et al., 1997; Hangen et al., 2005; Schmidt and Lin, 2008), in which break-through curve measurements have certain important implications regarding solute transport in the soil. These methods, however, cannot offer detailed information regarding flow and transport pathways and patterns, their spatial–temporal organizations, and their direct relationship with soil structural features.

In recent years, CT has provided an attractive tool for soil scientists to noninvasively observe soil structure (Warner et al., 1989; Gantzer and Anderson, 2002; Perret et al., 1999) and solute transport (Anderson et al., 1992; Peyton et al., 1994; Heijs et al., 1995; Perret et al., 2000). Three-dimensional visu-alization and quantification of soil macropores has been real-ized by synthesizing a series of two-dimensional CT images using certain algorithms (Capowiez et al., 1998; Pierret et al., 2002; Perret et al., 1999). Although CT was initially intended for viewing still images of scanned objects nondestructively, it can also be used to monitor changes in a process with time if repeated imaging is conducted during certain time inter-vals (Phogat and Aylmore, 1989; Hopmans et al., 1992). Clausnitzer and Hopmans (2000) quantified solute transport through glass beads using an industrial microfocus CT at a resolution of 86 μm. Perret et al. (2000) applied medical CT to isolate the soil matrix and macropore domains and monitored solute transport for 13 different locations within an intact soil column (7.7 cm in diameter and 85 cm in length). Anderson et al. (1992, 2003) developed a procedure to determine voxel porosity, the breakthrough curve, and pore water velocity with small soil cores (7.6 cm in diameter and 7.6 cm in length) using medical CT. This approach, however, requires a full replacement of water with solute tracer, a difficult process for large soil columns, especially when the soils are fine textured, have heterogeneous structure, or contain low-permeability layers.

Most of the published work has relied on medical CT, which has a limited spatial reso-lution (typically on the order of 1 mm) and a configuration that may prohibit vertical leaching experiments with large soil columns (Clausnitzer and Hopmans, 2000). The industrial CT scan-ner, on the other hand, has a higher resolution down to ~5 μm, and can be combined with real-time solute transport experiments using intact soil columns large enough to observe and quantify the dynamics of water, air, and solid interactions.

The objectives of this study were to use high-resolution industrial CT to: (i) recon-struct three-dimensional soil structure in a rela-tively large intact soil column; and (ii) quantify preferential tracer transport in real time and its dynamic relationships with soil structure (including various macropores). We used a com-bination of two techniques to quantify soil struc-ture and real-time solute transport: high-resolution industrial CT and digital radiograph (DR). The DR is another x-ray imaging technique that allows fast image collection and thus has great potential to observe flow processes effectively. It has been used to examine the bulk density profile of soil surface crusts (Bresson et al., 2004) and water movement through the soil (Maruyama et al., 2003). By directly observing and quantifying real-time solute transport in naturally structured soils with clear horizonation, as demonstrated in this study, we hope to better understand and quantify the impacts of soil structure and layering on preferen-tial flow and solute transport in an important agricultural soil, leading to new ways of modeling and prediction.

MATERIALS AND METHODS
The Soil Studied

Intact soil columns, 10 cm in diameter and 30 cm in height, were taken from The Pennsylvania State University's R.E. Larson Agricultural Research Center at Rock Springs in Centre County, Pennsylvania. The soil series is mapped as a Hagerstown silt loam (fine, mixed, semiactive mesic Typic Hapludalf) and the solum extends to >1 m. This is an important agricultural soil in the Ridge and Valley physiographic region of Pennsylvania. The sampled field has been in no-till since 1995 in a corn (*Zea mays* L.), soybean [*Glycine max* (L.) Merr.], and alfalfa (*Medicago sativa* L.) rotation. All plant residues were left in the field after each harvest. A backhoe was used to carefully push polyviniyl chlo-ride (PVC) pipes (10-cm inside diameter, 0.6-cm wall thickness) verti-cally and gradually into the soil. Five soil columns were collected and the one with the least possible disturbance due to sampling (based on multiple DRs taken at different angles of the columns, see Fig. 1) was
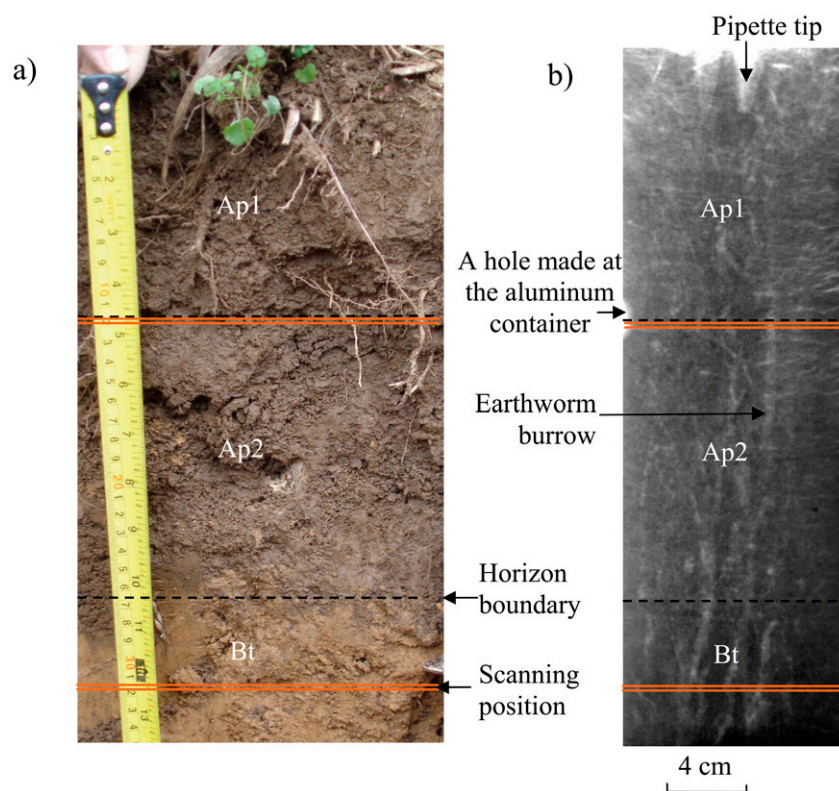

Fig. 1. The (a) soil profile and (b) digital radiograph (DR) of the intact soil column studied. Three soil horizons and their boundaries (black dashed lines), along with two selected scanning positions (red double lines), are indicated. In the DR, earthworm burrows are visible (light color channels).

Table 1. Basic properties of the soil column studied.

Horizon	Depth	Horizon boundary	Organic matter content	Particle size distribution			Roots	Soil structure	K_{sat}†	Bulk density	Total porosity
				Sand	Silt	Clay					
	cm		———— % ————						cm h^{-1}	g cm^{-3}	m^3 m^{-3}
Ap1	0–12	clear smooth	4.5	19.3	64.8	15.9	many fine and common medium roots	moderate medium subangular blocky	3.1	1.43	0.46
Ap2	12–23	abrupt smooth	3.5	17.1	68.1	14.8	common fine and few medium roots	moderate coarse platy	2.7	1.50	0.43
Bt	23–30+	–	1.9	22.9	51.7	25.4	common fine roots	moderate medium subangular blocky	2.1	1.61	0.39

† Saturated hydraulic conductivity.

selected for our experiment. The collected soil columns contained three soil horizons, each with a different structure and bulk density (Fig. 1, Table 1). Six small soil cores (5.5-cm diameter and 6.0-cm height) were also taken for each horizon to measure basic soil properties, including bulk density, organic matter content, texture, and saturated hydraulic conductivity (Table 1).
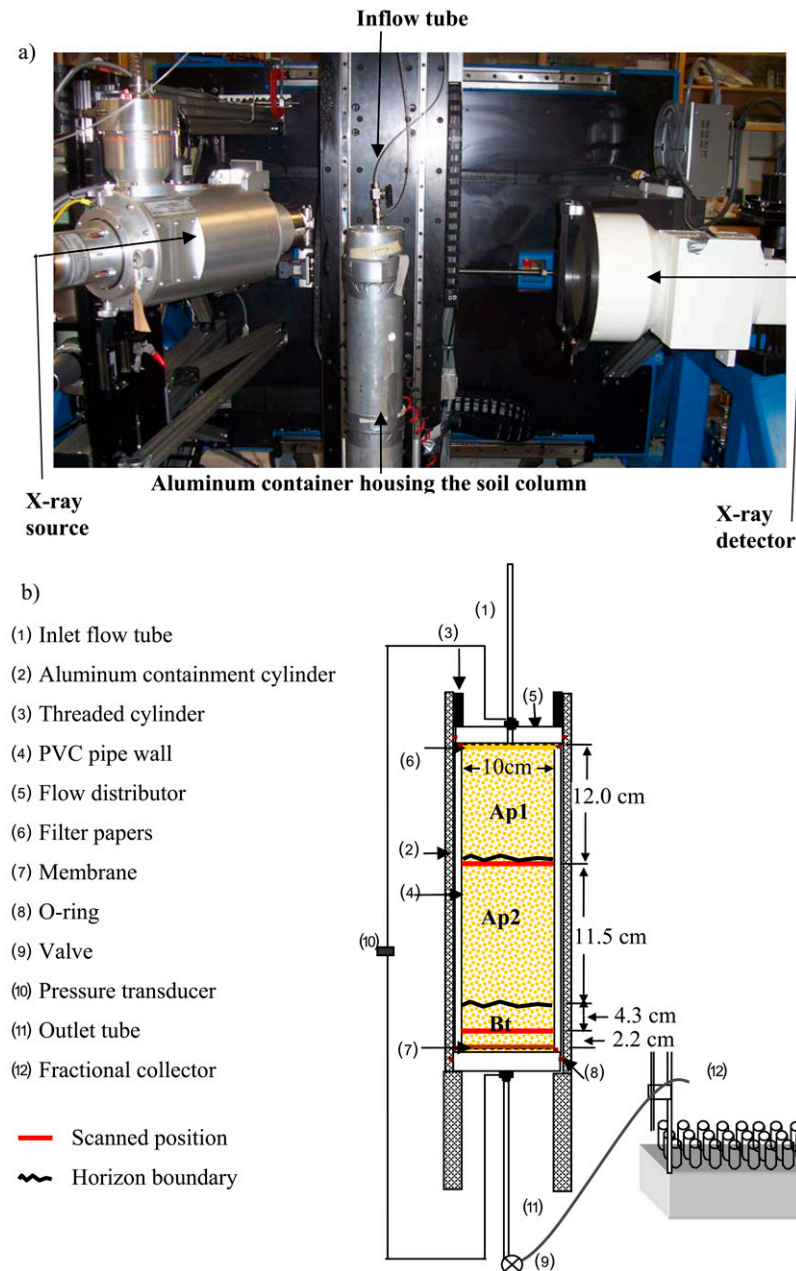
Industrial Computed Tomography

An industrial CT unit (OMNI-X model, Bio-Imaging Research, Lincolnshire, IL) was used for this experiment. This CT unit is a third-generation scanner, where the source and detector are fixed and the scanned object rotates (Fig. 2). The system has a 225 kV micro-focus x-ray generator and a 225-mm-diameter image intensifier. The highest resolution that can be obtained by the microfocus source is about 5 μm. The sample is rotated 360° to receive the x-ray beam (polychromatic) while the detector provides intensity views to the data acquisition computer. One rotation takes about 10 to 15 min, depending on the number of views taken. In this experiment, up to 41 slices were acquired in a single rotation with 2400 views. High-resolution images (1024 by 1024) were acquired as output in the computer system. Besides high-resolution cross-sectional CT scans, we also collected DRs using the same industrial CT to monitor the whole column during the experiment. The DRs were taken by collecting data from a single row of detectors while vertically moving the sample (without rotating it). This avoids the vertical geometric distortion that otherwise occurs when collecting a conventional two-dimensional image. The DRs and cross-sectional CT scans are fundamentally different: cross-sectional CT scans are used to obtain individual slices across the object, while the DRs reproduce a full two-dimensional projection of the whole object exposed to the x-ray and the x-ray attenuation value represents the effect of the object's density and thickness.

Experimental Procedure

The experiment setup is shown in Fig. 2. The soil column contained in the PVC pipe was housed in an aluminum cylindrical container (0.6-cm wall thickness) with a flow distributor at both ends of the soil column. A layer of filter paper was placed at the top of the soil column to distribute the solution evenly. A layer of pressure membrane (0.1-mm thick, 600-cm bubbling pressure, and 1.2-μm-diameter pore, with a conductivity of 0.2647 cm min^{-1} cm^{-2} at 1-cm hydraulic head, Soil Measurement System, Tucson, AZ) was placed at

Fig. 2. The computed tomography equipment setup showing (a) the actual aluminum containment cylinder, inflow tube, and x-ray source and detector, and (b) the diagram of the setup used for the solute transport experiment.

(1) Inlet flow tube
(2) Aluminum containment cylinder
(3) Threaded cylinder
(4) PVC pipe wall
(5) Flow distributor
(6) Filter papers
(7) Membrane
(8) O-ring
(9) Valve
(10) Pressure transducer
(11) Outlet tube
(12) Fractional collector

— Scanned position
〜 Horizon boundary

the bottom of the soil column. A threaded cylinder was tightened at the top of the aluminum container to compress the O-ring between the PVC pipe and flow distributor and create a seal at their interface. Three capped plastic pipette tips (1-cm diameter and 1.5-mL volume) filled with a 0.005 mol L^{-1} CaSO$_4$–water solution, air, and a 60 g L^{-1} KI solution, respectively, were inserted carefully into the top of the soil column to obtain their standard x-ray attenuation values (as references). The I$^-$ solution is a nonreactive tracer that has been successfully used to observe solute transport when coupling with x-ray CT. A relatively high concentration of I$^-$ (60 g L^{-1}) was used in the experiment to enhance the image quality (Perret et al., 2000; Clausnitzer and Hopmans, 2000); however, there may be some possible undesirable effects of introducing 60 g L^{-1} KI solution, such as density-driven flow and transport. A pressure transducer was connected to the both ends of the soil column to measure the pressure gradient throughout the experiment. An automatic fractional collector was used to collect the outlet flow at 1-min intervals within the first hour of the experiment and every 2 min thereafter.

The soil was satiated by pumping 0.005 mol L^{-1} CaSO$_4$ solution slowly (30 mL h^{-1}) into the soil column from the bottom. When water started to flow out of the tube at the top of the soil column, the pump rate was decreased to about 6 mL h^{-1} for about 24 h. This satiation process lasted for 2 d. The pressure difference between the two ends of the soil column and the flow rate were monitored to calculate the hydraulic conductivity of the entire soil column, which was 0.03 cm min^{-1} during the experiment. The whole soil column was then scanned at a resolution of 105.5 by 105.5 by 125.25 μm, which took 59 rotations and produced a total of 2419 slices. Two DRs were also taken at orthogonal angles to obtain the whole column images. After this scanning, 0.005 mol L^{-1} CaSO$_4$ solution was supplied at a constant flow rate of 6.5 mL min^{-1} (i.e., 0.08 cm min^{-1}) by pump from the top of the soil column. This flow rate was maintained throughout the experiment. When the outflow rate was constant, the 0.005 mol L^{-1} CaSO$_4$ solution was replaced by a 60 g L^{-1} KI solution. After introducing KI solution for 15 min, the pump and the valve at the outlet tube were turned off to stop the flow. Two selected critical positions in the soil column were scanned to observe the solute distribution (Fig. 1 and 2). The first position was located at the boundary between the Ap1 and Ap2 horizons, where preferential flow was expected; the second position was at about 2 cm above the bottom end of the soil column to avoid possible diffusion from the bottom flow distributor (Perret et al., 2000) but allowing the observation of the solute breakthrough in the Bt horizon and comparing with that measured in the Ap horizons. Each position was scanned for one rotation, with 41 slices representing a vertical thickness of 0.512 cm. In addition, two DRs were taken at orthogonal angles to obtain the whole column images. This process took about 27 min. It was assumed that all flow processes (diffusion, dispersion, convection, etc.) stopped during this 27-min time period (i.e., the limitation of the scanning speed was overcome by stopping the flow during the scanning). After this process, KI solution leaching was restarted and stopped again for scans at 30, 60, 90, 150, 230, 484, and 1374 min of accumulative flow time. At 1374 min, the whole soil column was scanned again to obtain the overall solute distribution in the column. By the end of the replacement experiment, about nine pore volumes of the KI solution had entered into the soil. The I$^-$ concentration in the effluent samples was measured using an I$^-$ electrode (Thermo Orion, Waltham, MA).

Data Analysis

Image analysis software AMIRA (TGS Inc., San Diego, CA) and ImageJ (Rasband, 2002) were used to analyze the data collected in this experiment.

Image Segmentation

There are many but no generally accepted definitions of a macropore (Beven and Germann, 1982; Chen, 1992; Perret et al., 1999). One main reason is that the definitions of macropores based on equivalent cylindrical diameter (ECD) are ambiguous and lack information about three-dimensional shape and function. Pores with ECD >1 mm have been commonly considered as macropores (Luxmoore et al., 1990; Perret et al., 1999). Ghezzehei and Or (2005) found a threshold of 0.6 mm in diameter to be a conservative upper limit for the applicability of capillaries dominated by Richards' equation. Schaap and van Genuchten (2006) analyzed 235 laboratory data from the UNSODA soil hydraulic database and suggested that pores with 0.075- and 0.75-mm ECD represented breakpoints of a two-element piecewise linear function between average scaled conductivities and pressure head. Notably, 0.075 mm is also the lower limit of very fine macropores defined by Brewer (1964) and adopted by the Soil Science Society of America (2006). It appears that the definition of macropores should consider both the data availability and the scale at which the problem is to be addressed. In this study, we considered the pores with ECD >0.75 mm as macropores.

Each voxel (a word combining *volume* and *pixel*) may have mixed components of air, water, and solid particles. In this study, the macropore network was segmented with voxel porosity >65% and ECD >0.75 mm. The image data were visually inspected to ensure that a reasonable threshold value was used based on the frequency distribution (histogram) of the attenuation coefficient (Peyton et al., 1994; Hopmans et al., 1992).

Calculation of Voxel Porosity and Solute Concentration

Spatially distributed porosity is useful to evaluate soil heterogeneity and quantify solute transport. In soils, three phases (solid, water, and air) contribute to the x-ray attenuation. When solutes in the soil water can be ignored, the x-ray attenuation value for a single voxel, CT(x,y,z) is

$$CT(x,y,z)=CT(x,y,z)_{solid}\left[1-\phi(x,y,z)\right] \\ +CT_{water}\phi(x,y,z)S_{water}+CT_{air}\phi(x,y,z)S_{air} \quad [1]$$

where CT(x,y,z)$_{solid}$ is the x-ray attenuation value for the solid of a given voxel; CT$_{water}$ and CT$_{air}$ are the x-ray attenuation values for water and air, respectively; $\phi(x,y,z)$ is the porosity of a given voxel; and S_{water} and S_{air} are the saturation ratios of water and air, respectively, in the voxel. The x-ray attenuation values of air, water, and 60 g L^{-1} KI solution were 394, 1271, and 1860, respectively, based on our standards.

To accurately quantify porosity, $\phi(x,y,z)$ for a given voxel in the soil, the optimal approach would be to scan the soil under two different conditions, totally saturated with water and completely dry. Alternatively, the soil can be scanned at either one of the above two conditions using dual energy (Rogasik et al., 1999). It is very difficult, however, for the soil to be fully saturated with water or to be completely dry (filled with air) under natural conditions. Such a total saturation or dryness may also induce swell–shrink for the soil with high clay content (such as the one used in this study). Besides, when the soil sample needs to be scanned twice, time and cost increase.

Since the KI solution displacement starts after the soil column is satiated with water, a linear relationship between the average x-ray attenuation value and I$^-$ concentration can be established when water in the soil is substituted by the KI solution. The relative concentration of KI solution, $C(x,y,z)_{rel}$, is defined as (Anderson et al., 1992)
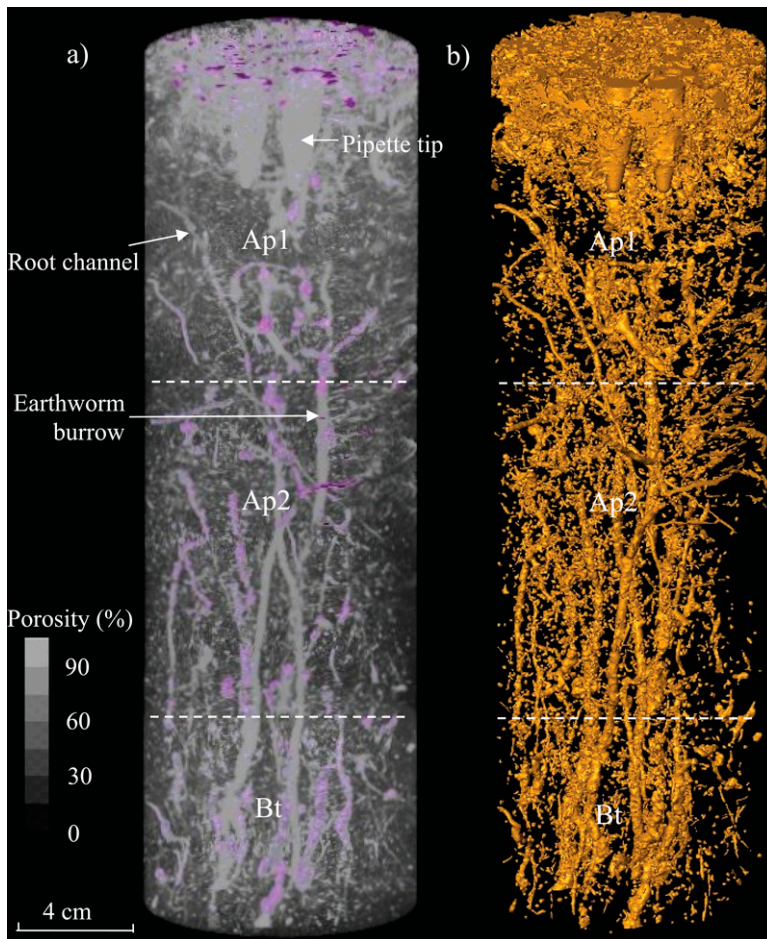
Fig. 3. A three-dimensional visualization of (a) the overall soil column porosity determined by the simplified method, along with entrapped air bubbles (in pink), and (b) the segmented macropore network (porosity >65%) in the soil column.
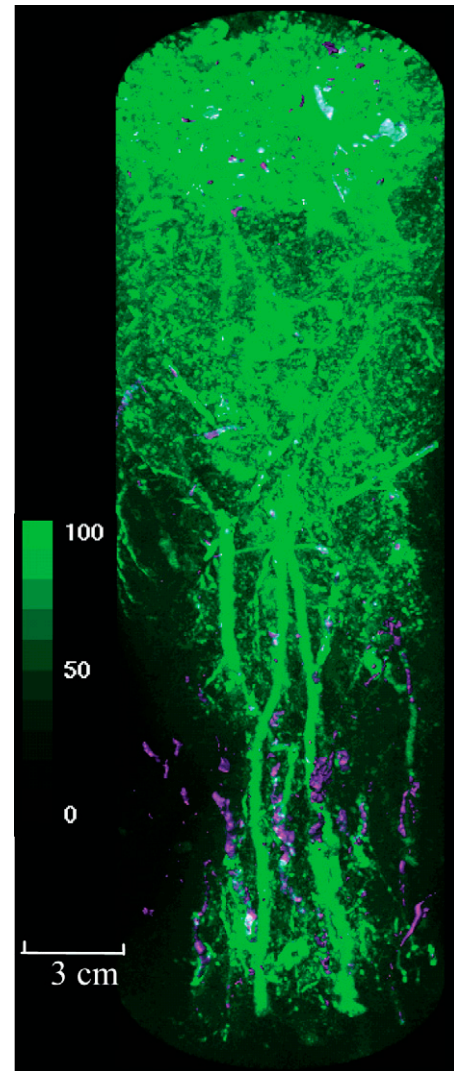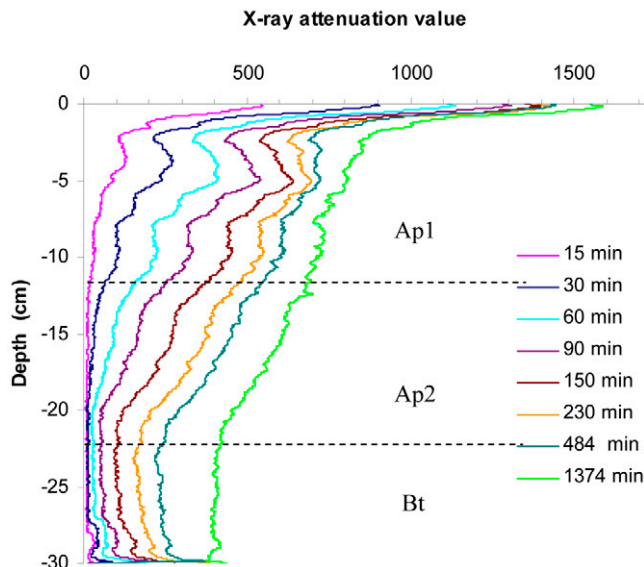

Fig. 8. The change of the x-ray attenuation value along the soil column with time, representing the change in solute mass distribution along the column depth.

$$C(x,y,z)_{rel} = \frac{CT(x,y,z,t) - CT(x,y,z,t=0)}{CT(x,y,z,T) - CT(x,y,z,t=0)} \qquad [2]$$

Fig. 15. A three-dimensional reconstruction of the solute mass distribution (in green) and the entrapped air distribution (in pink) at the end of the displacing process. Note that the solute mass was quantified by the ratio (in %) of the change in x-ray attenuation value during 1374 min [CT(x,y,z,t = 1374) − CT(x,y,z,t = 0)] to the x-ray attenuation value difference between the KI solution and water ($CT_{KI} - CT_{water}$).

where $CT(x,y,z,t)$ is the x-ray attenuation value for a voxel during breakthrough at time t; $CT(x,y,z,t = 0)$ is the x-ray attenuation value when the slice is satiated with water; and $CT(x,y,z,T)$ is the x-ray attenuation value when the soil is fully replaced by the solution. Similarly, the porosity can be calculated as (Anderson et al., 2003):

$$\phi(x,y,z) = \frac{CT(x,y,z,T) - CT(x,y,z,t=0)}{CT_{KI} - CT_{water}} \qquad [3]$$

where CT_{KI} is the x-ray attenuation value of a 60 g L^{-1} KI solution.

This method requires (i) a full replacement of water with solute, and (ii) a nonreactive solute. For a large structured soil (like the one used in this study), it is not easy to fully replace the water with solute, especially in the soil matrix. Consequently, we used a simplified approximation in this study to determine local porosity and concentration. If we assume that (i) the soil particle is homogeneous, that is, CT_{solid} is constant within a horizon, and (ii) when the soil is satiated, the air bubbles are only entrapped in large pores and are big enough to be identified using the images, that is, the voxels within the air bubbles are totally pore space (ϕ = 1), and those without air bubbles
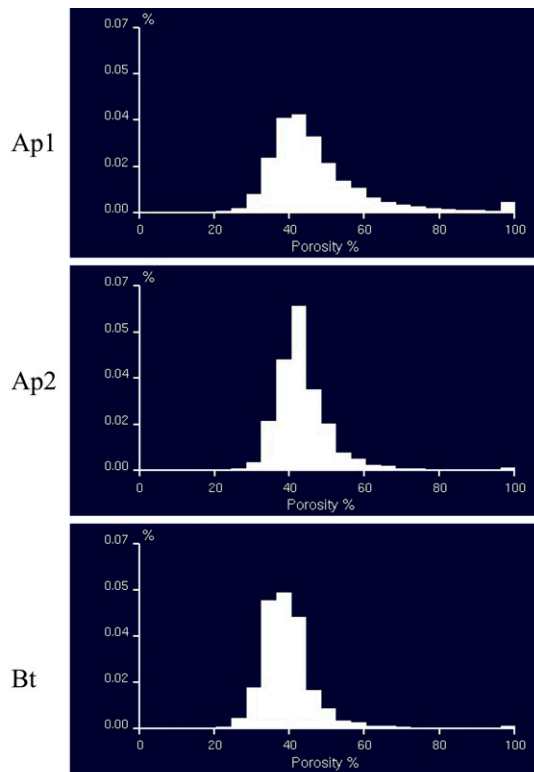
Fig. 4. The relative frequency distribution of the voxel porosity for the three soil horizons in the soil column studied.
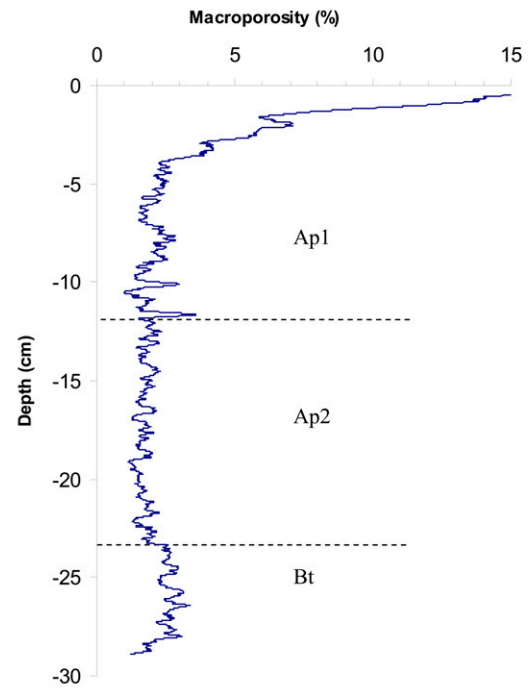

Fig. 5. Macroporosity distribution along the soil column depth as determined by the segmented macropores with equivalent cylindrical diameter >0.75 mm.

are fully filled with water (S_{water} = 1), then Eq. [1] can be applied to a given horizon (multivoxels) and written as

$$CT_{horizon} = CT_{solid\text{-}horizon}\left(1 - \phi_{horizon}\right) + CT_{water}\left(\phi_{horizon} - \phi_{air\text{-}horizon}\right) \quad [4]$$

where $CT_{horizon}$ is the average x-ray attenuation value for a given horizon, $\phi_{horizon}$ is the porosity of a given horizon, and $\phi_{air\text{-}horizon}$ is the volume percentage of entrapped air within a given horizon as determined from CT images. The x-ray attenuation value of solid for a given horizon, $CT_{solid\text{-}horizon}$, can be obtained by applying Eq. [4] to a region without air bubbles using known values of CT_{water}, ϕ_{air}, and $\phi_{horizon}$. The value of $\phi_{horizon}$ can be obtained from the measured soil bulk density data. Then, voxel porosity can be calculated by applying the following equation to each voxel for a given horizon using known $CT_{solid\text{-}horizon}$ and CT_{water} values:

$$\phi(x,y,z) = \frac{CT_{solid\text{-}horizon} - CT(x,y,z)}{CT_{solid\text{-}horizon} - CT_{water}} \quad [5]$$

Since a full replacement of water with solute was not obtained in this study, Eq. [2] cannot be used to obtain the relative concentration. Instead, the relative concentration for a given voxel was calculated as

$$C(x,y,z)_{rel} = \frac{CT(x,y,z,t) - CT(x,y,z,t=0)}{\left(CT_{KI} - CT_{water}\right)\phi(x,y,z)} \quad [6]$$

The median filter, a commonly used image processing method to reduce the noise while preserving the edge, was used to minimize the noise after subtracting the images taken at different times to quantify the solute concentration.

The first assumption stated above should be reasonable for an agricultural soil with few rock fragments,

which was the case in this study. Rogasik et al. (1999) used two energy levels to calculate the phase composition, i.e., solid, water, and air, of each voxel. They implicitly assumed CT_{solid} as a constant, although they also recognized that when at a microresolution, the variation in particle density cannot be ignored. For the second assumption, water enters more easily into the smaller pore space driven by capillarity. Likewise, the air tends to be trapped in larger pores. We recognize that some air bubbles may be trapped in smaller pores. For the voxels with trapped air, porosity may be underestimated and the relative concen-
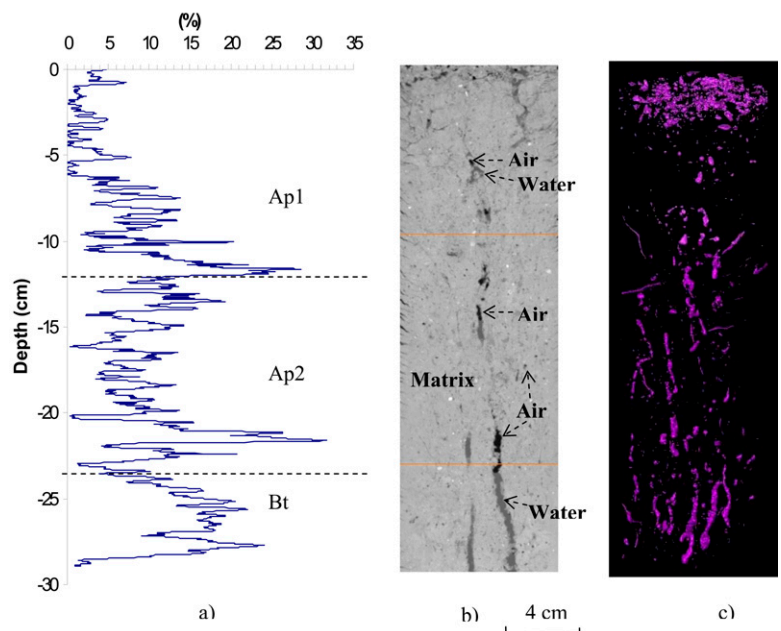

Fig. 6. The entrapped air distribution in the soil column before KI was introduced: (a) volume percentage of air-filled macropores as a function of soil depth, (b) a two-dimensional visualization of the entrapped air in the vertical profile (the dark areas are air pockets), and (c) a three-dimensional visualization of the entrapped air in the soil column (in pink).
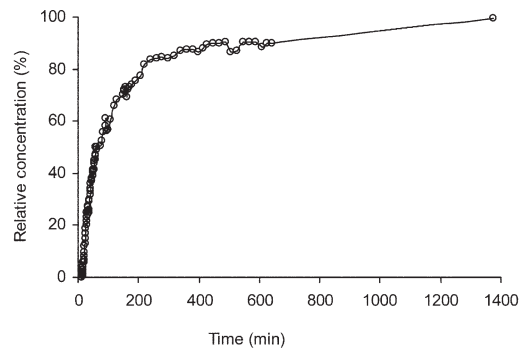
Fig. 7. The measured breakthrough curve of the effluent.

$$y = 44.343 \text{Ln}(x) - 183.77$$
$$R^2 = 0.9915$$

Fig. 9. The relationship between the change in the digital radiograph's x-ray attenuation value and the effluent relative concentration.

tration may be overestimated; however, we believe our approach will give a reasonable approximation of the overall picture of the soil structure and preferential movement of water, air, and tracer in this study.

RESULTS AND DISCUSSION
Reconstruction of Soil Structure, Pore Network, and Entrapped Air

Figure 3 shows a three-dimensional visualization of the spatial distribution of soil porosity determined by our simplified method, depicting the macropore network and entrapped air bubbles. Several types of macropores with distinct morphologies can be identified, including earthworm burrows, root channels, and interaggregate macropores. At the edge of the soil column, a small number of artificial fractures (parallel to the cross-section of the column) were detected. These were probably generated during the field sampling. The macropores formed by earthworm burrows and root channels were round in shape and highly continuous. Root channels were mainly distributed in the Ap1 and Ap2 horizons. Close to the boundary between the Ap1 and Ap2 horizons, root channels were more laterally extended. This is probably due to the dense platy structure of the plow pan (Ap2). Although earthworm burrows appeared in the Ap1 horizon, most of them were distributed in the Ap2 and Bt horizons. Earthworm burrows were vertically oriented; some parts of the burrows were refilled with loose soils. In contrast, the interaggregate pores were more randomly distributed in the soil and less continuous. It is also clear from Fig. 3 that there was no a single continuous macropore running from the top to the bottom of the soil column; instead, there was a complex network of macropores of varying sizes and continuities. Such a macropore network has critical impacts on flow and transport processes (discussed below).

The relative frequency distribution of voxel porosity, that is, the percentage of voxels with porosity in a certain range, is shown in Fig. 4 for each of the three soil horizons. Voxels with porosities from 35 to 55% dominated all three horizons (Fig. 4). The overall macroporosity in this soil column decreased dramatically from about 15% at the surface to about 2% at 4-cm depth, which is about the sowing depth in this soil (Fig. 5). Soil macroporosity then changed little (although with variation) with depth until reaching the Bt horizon, where macroporosity increased slightly to >2% (Fig. 5). Although the total macroporosity decreased in the Ap2 and Bt horizons, macropores in these two subsurface horizons were more vertically continuous (Fig. 3).

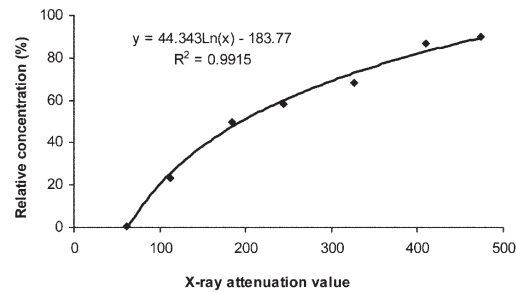Air was found to be entrapped more frequently at the top end of highly continuous macropores and in less continuous or isolated macropores in the Ap2 and Bt horizons, as well as in some artificial fractures along the column edge (Fig. 3 and 6). From Fig. 6a, we can see that the ratio of macropores filled with air increased with soil depth. The entrapped air made up 9.8, 11.5, and 18.5% of the macropore volume in the Ap1, Ap2, and Bt horizons, respectively. Thus, the hydraulic conductivity measured under this condition is indeed "quasi-saturated" or "satiated" (meaning that not 100% of the pore space was filled with water). Earlier studies by Faybishenko (1995), Chapuis (2004), and Sakaguchi et al. (2005) showed that entrapped air could occupy up to 15% of the bulk soil volume and greatly influenced hydraulic conductivity. Faybishenko (1995) described three stages in temporal behavior of entrapped air and quasi-saturated soil hydraulic conductivity, and proposed a power law and an exponential relationship to describe quasi-saturated hydraulic conductivity as a function of the entrapped air content. Further research is needed, however, on how air is entrapped and changed under different conditions and how to precisely determine the amount of entrapped air in a complex soil pore network.

Quantification of Solute Transport and Entrapped Air

The effluent breakthrough curve showed a quick response when the tracer was first introduced and a very long tail, indicating the occurrence of preferential flow and a gradual interaction between the macropore and matrix domains (Fig. 7). The relative concentration of the effluent quickly reached 50% after 60 min, but after 200 min the relative concentration increased very slowly. Even after 1374 min, the water was not completely replaced by the tracer (99.7% relative concentration).

The solute transport with time within the whole soil column can be obtained by subtracting the DRs taken at different times during the experiment (Fig. 8). The change in the x-ray attenuation value with depth is linearly correlated to the solute mass distribution along the soil column. In the soil column studied, the change in the x-ray attenuation value decreased rapidly in the top 3 cm and decreased more slowly and nearly linearly from 3 cm to the top of the Bt horizon, and then remained relatively constant in the Bt horizon (Fig. 8).

An exponential relationship was found between the change in average x-ray attenuation value of the DRs and the relative concentration of effluent solute tracer (Fig. 9). This relationship was used to quantify the solute transport processes (Fig. 10 and 11). As visualized in Fig. 10 and 11, the solute moved preferentially through cracks at the surface in the beginning, and then quickly reached some macropores in the subsurface. Some earthworm burrows and root channels were highly active in solute
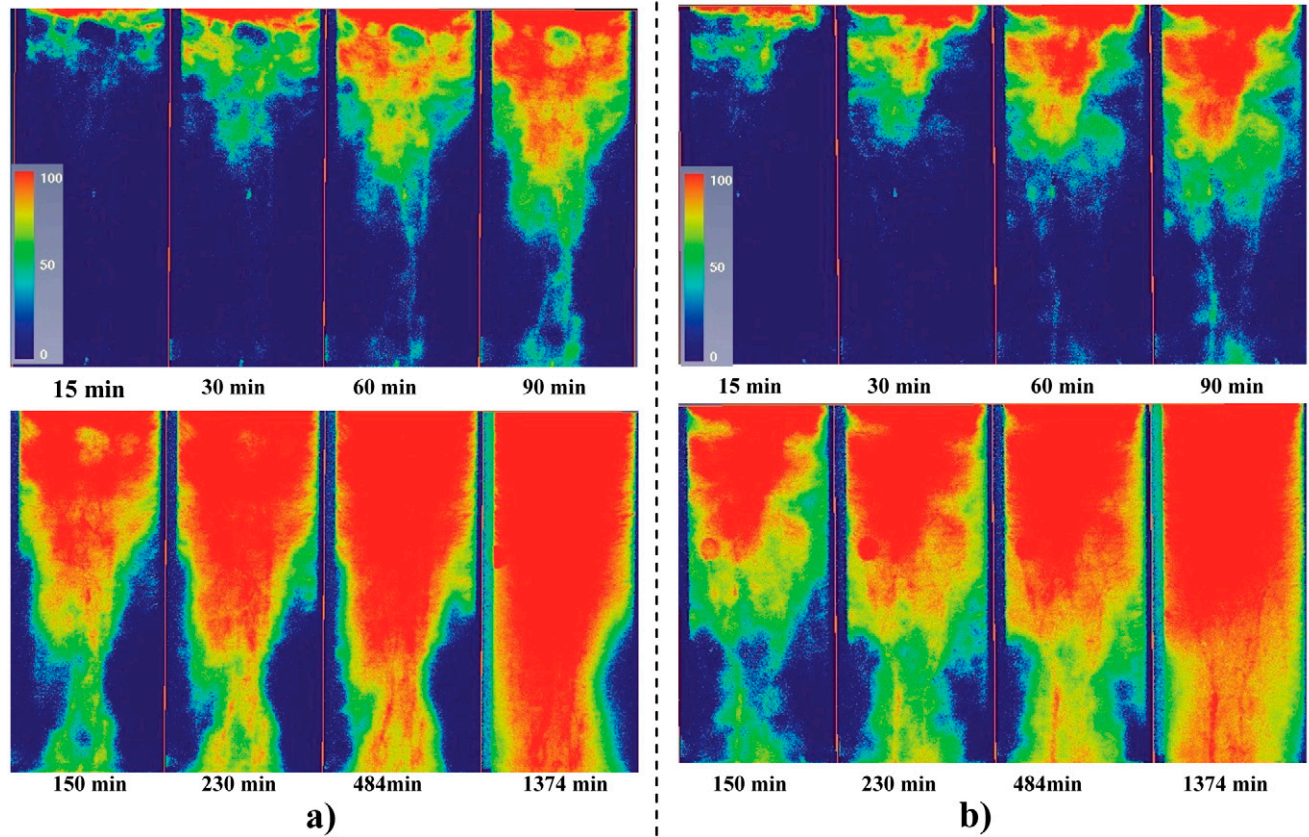
Fig. 10. The solute transport with time based on the relationship between the change in the digital radiograph's x-ray attenuation value and effluent relative concentration for the entire soil column scanned at two angles: accumulative solute concentration (%) at (a) 0° and (b) 90°.
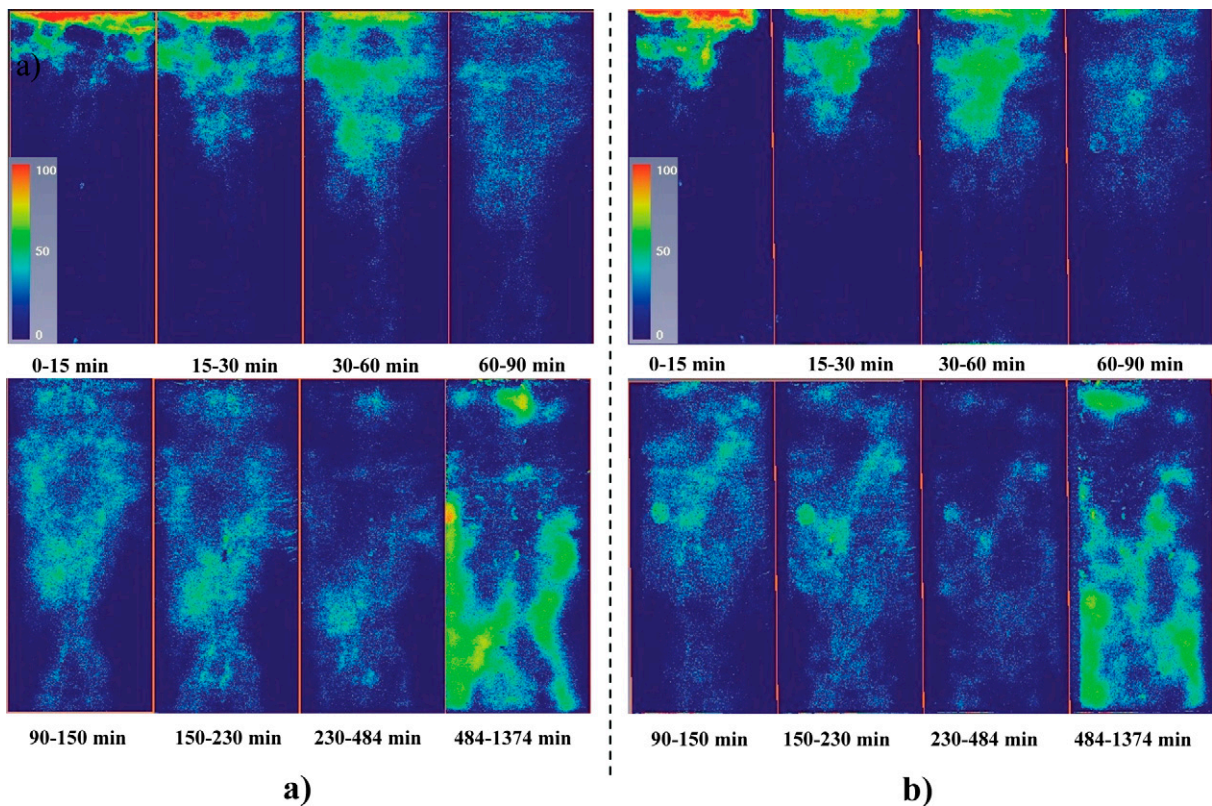

Fig. 11. The change in solute concentration (%) during the time interval indicated for the entire soil column scanned at two angles: (a) 0° and (b) 90°.

transport because of their high continuity and low tortuosity. Once the downward preferential flow had been initiated, lateral expansion of the solute from the preferential flow pathways to the surrounding matrix began. After 230 min, the main prefer-
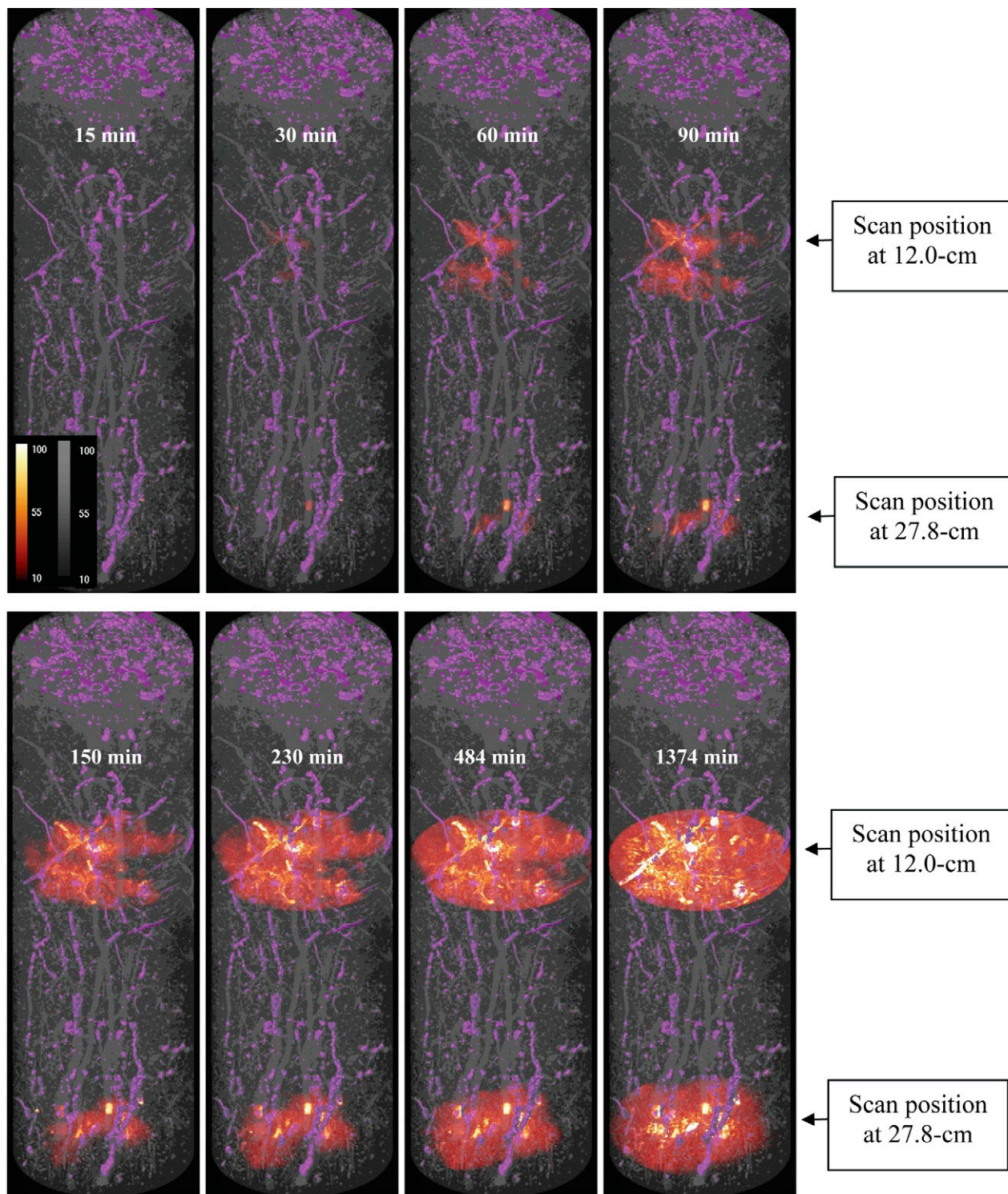
Fig. 12. The solute distribution (brownish color, in relative concentration [%]) at two scanned positions of 12.0- and 27.8-cm depth in the soil column with time. The gray color indicates soil porosity (%) and the pink color indicates the entrapped air bubbles.

ential flow pathways were almost fully filled with the KI solution (Fig. 11). A gradual lateral expansion then started to dominate the transport process, even though vertical movement of solute could still be detected (Fig. 11). Even after about 23 h (1374 min), pores in the soil matrix were still not completely filled by the KI solution, especially in the Bt horizon. Since the DR is a two-dimensional projection of the soil column exposed to x-ray, the pixel-based concentration was the overlapped effect of solute transport in the soil along a line at a given depth. Thus cau-

tion should be exercised when linking the results from the two-dimensional DR images to the three-dimensional soil structure and solute distribution. The accuracy of the quantified relative concentration using the DRs is therefore limited. Nevertheless, the DR is still an effective and economical means to nondestructively and quickly observe and quantify solute transport in real time along the entire soil column.

Time series data of the two CT-scanned key positions (12.0- and 27.2-cm depths) provided the details about how

macropores and the matrix interacted during solute transport (Fig. 12). At the 12-cm depth, the solute tracer preferentially moved through some root channels and earthworm burrows; however, preferential flow also occurred in some areas without obvious macropores at the 12-cm depth (Fig. 12). There were highly continuous and effective macropores below them, suggesting the impact of large continuous macropores on the soil below the 12-cm depth. Because of the higher porosity in the upper portion of the soil column and longer interaction time, there was a higher degree of interaction between the macropore and matrix domains than that in the lower portion of the soil column. Compared with the upper position, the tracer showed up first in continuous root channels and earthworm burrows at the 27.7-cm depth. Even though some macropores contained trapped air, flow still occurred along these openings. In contrast, even without entrapped air, some macropores in the subsurface horizon were not active in solute transport (Fig. 12). Similarly, Luxmoore et al. (1990) showed that not all macropores were hydrologically active in the forest watershed that they studied.

After dividing the soil into the matrix and macropore domains, breakthrough curves (BTCs) of the macropore and matrix domains were calculated using the time series of CT images at the two scanned positions (Fig. 13). The BTCs for both the macropore and the matrix domains at the two scanned positions were below the measured effluent BTC, indicating that the flux concentration was greater than the resident concentration and that preferential flow was occurring (Zhang et al., 2006). The deviation of these calculated BTCs from the actual effluent BTC implies that the macropore network in itself cannot be considered simply as preferential flow pathways. It is the hydrologic connectivity of macropores that is essential. Compared with the scanned position at the 12-cm depth, macropore and matrix BTCs for the second scanned position were further apart (Fig. 13), suggesting that more pronounced preferential flow occurred in the deeper soil.

Figure 14 shows BTCs at selected specific points (5 by 5 voxels in the scanned cross-section of the position at the 27.8-cm depth). Point 1 represents a macropore; Point 2 was between a macropore and the matrix (i.e., the interface); while Points 3 and 4 represented the soil matrix. Sequential initialization of solute transport at these three types of positions was observed. The concentration decrease that occurred at Points 2 and 4 could have resulted from noise. With the voxel-based BTC, the solute travel time to a voxel could be determined.
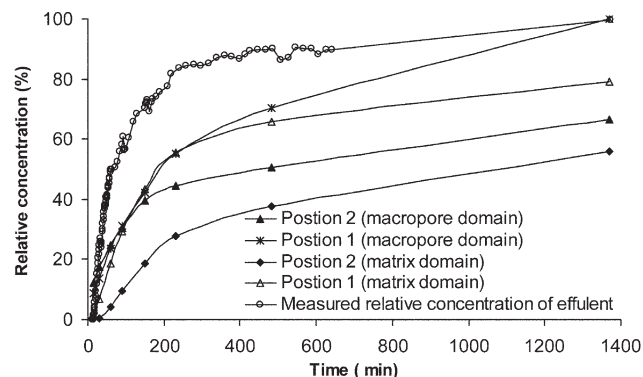

Fig. 13. Breakthrough curves of the macropore and matrix domains at two scanned positions of 12.0- (Position 1) and 27.8-cm depth (Position 2) in the soil column studied.

The solute travel time to a voxel was considered the time when relative concentration was equal to 0.5 (Anderson et al., 1992). A velocity was calculated using the travel time and the vertical distance from the soil surface. The pore velocity differed considerably for different points. For Points 1, 2, and 3 in Fig. 14, the pore velocities were 0.68, 0.47, and 0.06 cm min^{-1}, respectively. For Point 4, the concentration never reached 50%, so the velocity was <0.02 cm min^{-1}.
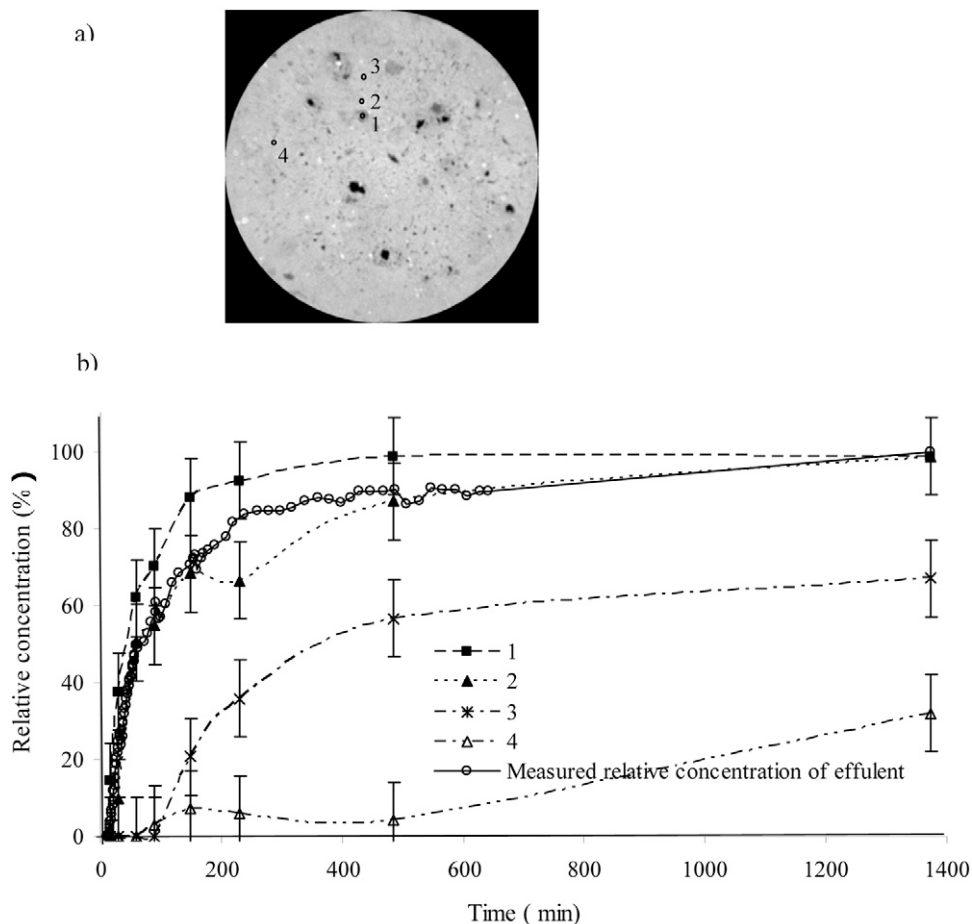

Fig. 14. (a) Selected points in the cross-section at 27.8-cm depth in the soil column and (b) their point-specific breakthrough curves. Point 1 is a macropore, Point 2 is adjacent to a macropore, and Points 3 and 4 are soil matrix. Error bars indicate a variation of ±26 in x-ray attenuation value, corresponding to about ±5% variation in relative concentration.

The three-dimensional visualization of the solute mass distribution at 1374 min displayed a pattern similar to that revealed by the DRs, that is, the solute distribution in the Ap1 horizon was more evenly distributed, while that in the Ap2 and Bt horizons were more heterogeneous or preferentially oriented (Fig. 15). Such a pattern matches the conceptualization of preferential flow zones in a soil profile, as suggested by Flühler et al. (1996) and Kim et al. (2005), that is, there is a distribution or an induction zone near the soil surface and a conveyance or transmission zone below it. The overall match between the DRs (Fig. 10 and 11) and the CT images also demonstrated the usefulness of the DR imaging technique as used in this study.

Entrapped air movement was observed during the solute transport process in this study. During the entire experiment, some entrapped air bubbles gradually decreased in size with time, and some disappeared eventually (e.g., compare Fig. 6c and 15). There was an obvious relationship between the elapsed time and the reduced air volume in the soil column. The air volume reduction also varied with the soil depth. Air volume percentage decreased 60.3% in the Ap1 horizon, 52.6% in the Ap2 horizon, and 24.6% in the Bt horizon during the 23-h experiment. Some localized increase in air volume in the subsurface indicated a downward movement of air. With the differential pressure transducer data, we found that the pressure difference between the two ends of the soil column decreased by about 10% from the beginning to the end of our experiment. Experimentally, a vacuum or CO_2 could be used to reach a more fully saturated state and avoid the complexity of flow with trapped air. We believe, however, that our experiment reflects the natural flow condition in the field, as air is often entrapped by natural rainfall or irrigation water and thus influences flow and transport processes in field soils.

SUMMARY AND CONCLUSIONS

High-resolution industrial CT has allowed reconstruction, visualization, and quantification of soil structure and solute transport in a relatively large intact soil column. Besides cross-sectional scans, digital radiography was also shown to be an effective tool to nondestructively characterize solute transport in real time when combined with a solute tracer. The potential of digital radiography has been underutilized in past CT-related research.

Different kinds of macropores with distinct morphologies (such as earthworm burrows, root channels, and interaggregate macropores) and their different functions in solute transport were observed, which varied with soil depth or horizon. Only portions of the macropores, especially the highly continuous biogenetic macropores in the subsurface, were active in transporting the solute, in part because of entrapped air that made up 9.8, 11.5, and 18.5% of the macropore volume in the Ap1, Ap2, and Bt horizons, respectively. Air movement was also observed during the flow and transport process under the quasi-saturated flow condition. Voxel-based breakthrough curves determined with real-time solute transport data can be further used to infer local solute dispersion parameters and test current models such as dual-permeability models, and to estimate water flow and solute transport in heterogeneous soils.

This study illustrates the complex nature of preferential flow dynamics in a structured soil. Preferential flow pathways in the intact structured soil consist of a complex network of various macropores, including earthworm burrows, root channels, interaggregate macropores, and even mesopores or micropores in the soil matrix. No macropores were continuous from the top to the bottom of the soil column, and some macropores were not effective for flow and transport due to air entrapment or hydrologic discontinuities. This result is similar to the in situ finding of Noguchi et al. (1999), who found that about 70% of the macropores (≥ 2 mm) were discontinuous (dead end) in an 8-cm-long section in a forest hillslope and only 1% of all macropores continued for 40 cm. Therefore, the macropore network by itself cannot simply be equated to a preferential flow network. Based on field investigations, including tracer tests, Sidle et al. (2001) considered preferential flow systems in natural soils to consist of more than simply interconnected macropore elements. They proposed the concept of linking individual short macropores via a series of nodes, which may be switched off or on and expand or shrink depending on local soil and antecedent moisture conditions. Such a concept may lead to a new way of modeling and predicting preferential flow dynamics in relation to soil structure in the real world.

REFERENCES
Anderson, S.H., R.L. Peyton, J.W. Wigger, and C.J. Gantzer. 1992. Influence of aggregate size on solute transport as measured using computed tomography. Geoderma 53:387–398.

Anderson, S.H., H. Wang, R.L. Peyton, and C.J. Gantzer. 2003. Estimation of porosity and hydraulic conductivity from x-ray CT-measured solute breakthrough. p. 135–150. In F. Mees et al. (ed.) Applications of x-ray computed tomography in the geosciences. Geol. Soc., London.

Beven, K., and P. Germann. 1982. Macropores and water flow in soils. Water Resour. Res. 18:1311–1325.

Boll, J., J.S. Selker, G. Shalit, and T.S. Steenhuis. 1997. Frequency distribution of water and solute transport properties derived from pan sampler data. Water Resour. Res. 33:2655–2664.

Bresson, L.M., C.J. Moran, and S. Assouline. 2004. Use of bulk density profiles from x-radiography to examine structural crust models. Soil Sci. Soc. Am. J. 68:1169–1176.

Brewer, R. 1964. Fabric and mineral analysis of soils. John Wiley & Sons, New York.

Capowiez, Y., A. Pierret, O. Daniel, P. Monestiez, and A. Kretzschmar. 1998. 3D skeleton reconstructions of natural earthworm burrow systems using CAT scan images of soil cores. Biol. Fertil. Soils 27:51–59.

Chapuis, R.P. 2004. Permeability tests in rigid-wall permeameters: Determining the degree of saturation, its evolution, and its influence on test results. Geotech. Test. J. 27:304–313.

Chen, C. 1992. Simulation of water and chemicals in macropore soils. Part 1. Representation of the equivalent macropore influence and its effect on soil water flow. J. Hydrol. 130:105–126.

Clausnitzer, V., and J.W. Hopmans. 2000. Pore-scale measurements of solute breakthrough using microfocus x-ray computed tomography. Water Resour. Res. 36:2067–2079.

Faybishenko, B.A. 1995. Hydraulic behavior of quasi-saturated soils in the presence of entrapped air: Laboratory and field experiments. Water Resour. Res. 31:2421–2435.

Feyen, H., H. Wunderli, H. Wydler, and A. Papritz. 1999. A tracer experiment to study flow paths of water in a forest soil. J. Hydrol. 225:155–167.

Feyen, J., D. Jacques, A. Timmerman, and J. Vanderborght. 1998. Modelling water flow and solute transport in heterogeneous soils: A review of recent approaches. J. Agric. Eng. Res. 70:231–256.

Flühler, H., W. Durner, and M. Flury. 1996. Lateral solute mixing processes: A key for understanding field-scale transport of water and solutes. Geoderma 70:165–183.

Flury, M., and N.N. Wai. 2003. Dyes as tracers for vadose zone hydrology. Rev. Geophys. 41(1):1002, doi:10.1029/2001RG000109.

Gantzer, C.J., and S.H. Anderson. 2002. Computed tomographic measurement of macroporosity in chisel-disk and no-tillage seedbeds. Soil Tillage Res. 64:101–111.

Gerke, H.H., and M.G. Schaap. 1993. A dual-porosity model for simulating the preferential movement of water and solutes in structured porous media. Water Resour. Res. 29:305–319.

Germann, P. 1985. Kinematic wave approach to infiltration and drainage into and from soil macropores. Trans. ASAE 28:745–749.

Ghezzehei, T.A., and D. Or. 2005. Liquid fragmentation and intermittent flow regimes in unsaturated fractures. Water Resour. Res. 41:W12406, doi:10.1029/2004WR003834.

Gwo, J.P., P.M. Jardine, G.V. Wilson, and G.T. Yeh. 1995. A multiple-pore-region concept to modeling mass transfer in subsurface media. J. Hydrol. 164:217–237.

Hangen, E., H.H. Gerke, W. Schaaf, and R.F. Huttl. 2005. Assessment of preferential flow processes in a forest-reclaimed lignitic mine soil by multicell sampling of drainage water and three tracers. J. Hydrol. 303:16–37.

Heijs, A.W.J., J. Delange, J.F.T. Schoute, and J. Bouma. 1995. Computed tomography as a tool for nondestructive analysis of flow patterns in macroporous clay soils. Geoderma 64:183–196.

Hopmans, J.W., T. Vogel, and P.D. Koblik. 1992. X-ray tomography of soil-water distribution in one-step outflow experiments. Soil Sci. Soc. Am. J. 56:355–362.

Kim, Y.J., C.J.G. Darnault, N.O. Bailey, J.Y. Parlange, and T.S. Steenhuis. 2005. Equation for describing solute transport in field soils with preferential flow paths. Soil Sci. Soc. Am. J. 69:291–300.

Köhne, J.M., and B.P. Mohanty. 2005. Water flow processes in a soil column with a cylindrical macropore: Experiment and hierarchical modeling. Water Resour. Res. 41:W03010, doi:10.1029/2004WR003303.

Lin, H.S., J. Bouma, L.P. Wilding, J.L. Richardson, M. Kutílek, and D.R. Nielsen. 2005. Advances in hydropedology. Adv. Agron. 85:1–90.

Luxmoore, R.J., P.M. Jardine, G.V. Wilson, J.R. Jones, and L.W. Zelazny. 1990. Physical and chemical controls of preferred path flow through a forested hillslope. Geoderma 46:139–154.

Maruyama, T., A. Tada, K. Iwama, and H. Horino. 2003. Direct observation of soil water movement through soil macropores using soft x-rays and stereographing. Soil Sci. 168:119–127.

Noguchi, S., Y. Tsuboyama, R.C. Sidle, and I. Hosoda. 1999. Morphological characteristics of macropores and the distribution of preferential flow pathways in a forested slope segment. Soil Sci. Soc. Am. J. 63:1413–1423.

Perret, J., S.O. Prasher, A. Kantzas, and C. Langford. 1999. Three-dimensional quantification of macropore networks in undisturbed soil cores. Soil Sci. Soc. Am. J. 63:1530–1543.

Perret, J., S.O. Prasher, A. Kantzas, and C. Langford. 2000. A two-domain approach using CAT scanning to model solute transport in soil. J. Environ. Qual. 29:995–1010.

Peyton, R.L., C.J. Gantzer, S.H. Anderson, B.A. Haeffner, and P. Pfeiffer. 1994. Fractal dimension to describe soil macropore structure using x-ray computed tomography. Water Resour. Res. 30:691–700.

Phogat, V.K., and L.A.G. Aylmore. 1989. Evaluation of soil structure by using computer-assisted tomography. Aust. J. Soil Res. 27:313–323.

Pierret, A., Y. Capowiez, L. Belzunces, and C.J. Moran. 2002. 3D reconstruction and quantification of macropores using x-ray computed tomography and image analysis. Geoderma 106:247–271.

Rasband, W. 2002. ImageJ: Image processing and analysis in Java. Available at rsb.info.nih.gov/ij/index.html (verified 8 May 2008). Research Services Branch, Natl. Inst. of Health, Bethesda, MD.

Rogasik, H., J.W. Crawford, O. Wendroth, I.M. Young, M. Joschko, and K. Ritz. 1999. Discrimination of soil phases by dual energy x-ray tomography. Soil Sci. Soc. Am. J. 63:741–751.

Sakaguchi, A., T. Nishimura, and M. Kato. 2005. The effect of entrapped air on the quasi-saturated soil hydraulic conductivity and comparison with the unsaturated hydraulic conductivity. Vadose Zone J. 4:139–144.

Schaap, M.G., and M.Th. van Genuchten. 2006. A modified Mualem–van Genuchten formulation for improved description of the hydraulic conductivity near saturation. Vadose Zone J. 5:27–34.

Schmidt, J.P., and H.S. Lin. 2008. Water and bromide movement in conventionally tilled and no-tilled corn: Contrasting results from pan and wick lysimeters. Commun. Soil Sci. Plant Anal. 39:108–123.

Sidle, R.C., S. Noguchi, Y. Tsuboyama, and K. Laursen. 2001. A conceptual model of preferential flow systems in forested hillslopes: Evidence of self-organization. Hydrol. Processes 15:1675–1692.

Šimunek, J., N.J. Jarvis, M.Th. van Genuchten, and A. Gardenas. 2003. Review and comparison of models for describing non-equilibrium and preferential flow and transport in the vadose zone. J. Hydrol. 272:14–35.

Soil Science Society of America. 2006. Pore size classification. Available at www.soils.org/sssagloss/pdf/table2.pdf (verified 8 May 2008). SSSA, Madison, WI.

van Genuchten, M.Th., and P.J. Wierenga. 1976. Mass transfer studies in sorbing porous media: 1. Analytical solutions. Soil Sci. Soc. Am. J. 40:473–481.

Vogel, H.J. 2000. A numerical experiment on pore size, pore connectivity, water retention, permeability, and solute transport using network models. Eur. J. Soil Sci. 51:99–105.

Warner, G.S., J.L. Nieber, I.D. Moore, and R.A. Geise. 1989. Characterizing macropores in soil by computed tomography. Soil Sci. Soc. Am. J. 53:653–660.

Young, I.M., J.W. Crawford, and C. Rappoldt. 2001. New methods and models for characterizing structural heterogeneity of soil. Soil Tillage Res. 61:33–45.

Zhang, Y., B. Baeumer, and D.A. Benson. 2006. Relationship between flux and resident concentrations for anomalous dispersion. Geophys. Res. Lett. 33:L18407, doi:10.1029/2006GL027251.